Patterned Immobilization of Antibodies in Mechanically Induced Cracks

Ting Cao,[†] Anfeng Wang,[†] Xuemei Liang,[†] Haiying Tang,[†] Gregory W. Auner,[‡] Steven O. Salley,[†] and K.Y. Simon Ng*[,†]

Department of Chemical Engineering and Materials Science and Department of Electrical and Computer Engineering, Wayne State University, 5050 Anthony Wayne Drive, Detroit, Michigan 48202

Received: November 20, 2007; In Final Form: December 17, 2007

A new approach of chemically immobilizing antibody within a pattern based on thin-film cracking is presented. An adjustable pattern width is achieved with resolutions varied from nano- to microscale by using loading stress on thin-film coated elastomer substrate in both one and two dimensions. By introduction of solution or chemical vapor deposition approaches, antibodies were covalently immobilized in the channels. To demonstrate the bioactivity, specificity, and response rate of antibody patterned structure, scanning electron microscopy was used to enumerating bacteria. The chemically coupled antibody is found to retain its specificity when incubated with different bacteria solutions. Trichloro(1*H*,1*H*,2*H*,2*H*-perfluoroctyl)silane coating on nonsensing regions exhibits a distinguished bacteria-resistant function that is beneficial for providing a low intrinsic background signal in detection. This technique shows a great potential for applications in the fields of sensing and tissue engineering.

Introduction

Early detection of pathogens such as biological toxins, bacteria, viruses, and fungi is of importance in the areas of public safety, military applications, and homeland security. In the medical community, it can be applied in cancer diagnosis and treatment,[1] molecular classification of disease,[2] and tissue proteomics. Highly sensitive and selective biosensors with fast response rates are extremely desirable. Compared to conventional techniques, the fabrication of micro- or nanoscale structures is a very promising technique for chemical and biochemical sensors. In addition, this technique allows for the creation of a miniaturized biosensor.[3]

Different techniques have been developed to generate patterns at the nanometer scale, including photolithography, writing with a rigid stylus[4] or a beam of energetic particles,[5,6] and molecular self-assembly.[7,8] Although some of these methods perform extremely well for fabrication requirements, there are some significant limitations. For instance, photolithography can only be applied to a few functional materials such as photoresists;[9] writing requires focused beams of energetic particles to generate patterns in appropriate resist materials;[5,10] molecular self-assembly is triggered by the interaction between molecules such as electrostatic, hydrophobic, van der Waals's interaction, as well as a hydrogen bonding.[11] Also, few of these methods can provide patterns that range from 100 to 3000 nm,[12] and they are not convenient for fabrication.

Recently thin-film fractures have been systematically investigated as a method to generate nanoscale structures[12−14] by subjecting them to high residual stresses during the fabrication process.[15] Two crucial features make this technique attractive. First, the pattern can be varied from nano- to microscale using simple and inexpensive procedures. Second, the pattern can be generated over a few square centimeters. This novel and effective chemical−mechanical technique was reported to fabricate reconfigurable protein matrices, in which the protein patterns were created with adjustable width.[12]

However, the limitation of this method is that bioligands directly patterned depend on their affinity to the side-walls of cracks. It is well-known that physisorption of proteins to a surface is very sensitive to environmental conditions and the process is reversible. Surface immobilization of biomolecules with a specific orientation is critical for sensing substrates since this determines the primary properties of the biosensor such as sensitivity and selectivity. Also, Weimer et al. reported that, with the help of spacers, a better capture efficiency can be obtained than with direct immobilization.[16] With the greater flexibility of a spacer, the steric interference may be reduced significantly. Thus, in the present study, spacers were used as part of antibody immobilization.

Besides the pattern fabrication and enhanced protein binding properties, another important concern in creating sensing substrates is to have a low intrinsic background signal within a given detection system. Thus the requirement for sensing substrates includes that the inert region would prevent the adsorption of protein and adhesion of analytes such as proteins or cells. A number of methods have been extensively studied to generate passive surfaces, including carbohydrates,[17,18] poly(ethylene glycol),[19] pluronics, or proteins such as albumin.[20] Although they all appear to resist protein adsorption, few have been proven to suppress bacterial adhesion.[21,22] We reported that fluoroalkylsilane surfaces significantly reduced not only bacteria (*Escherichia coli* and *Staphylococcus epidermidis*)[23,24] but also neural cells.[25]

In this study, the objective is to use a thin-film cracking method and covalent binding to fabricate protein patterns and to provide a low intrinsic background signal sensing system through formation of a bacteria- and cell-resistant monolayer. To this end, patterns were created on silicone rubber substrates

* To whom correspondence should be addressed. E-mail: sng@wayne.edu. Phone: 313-577-3805. Fax: 313-577-3810.

[†] Department of Chemical Engineering and Materials Science, Wayne State University.

[‡] Department of Electrical and Computing Engineering, Wayne State University.

10.1021/jp711070k CCC: $40.75
Published on Web 02/13/2008

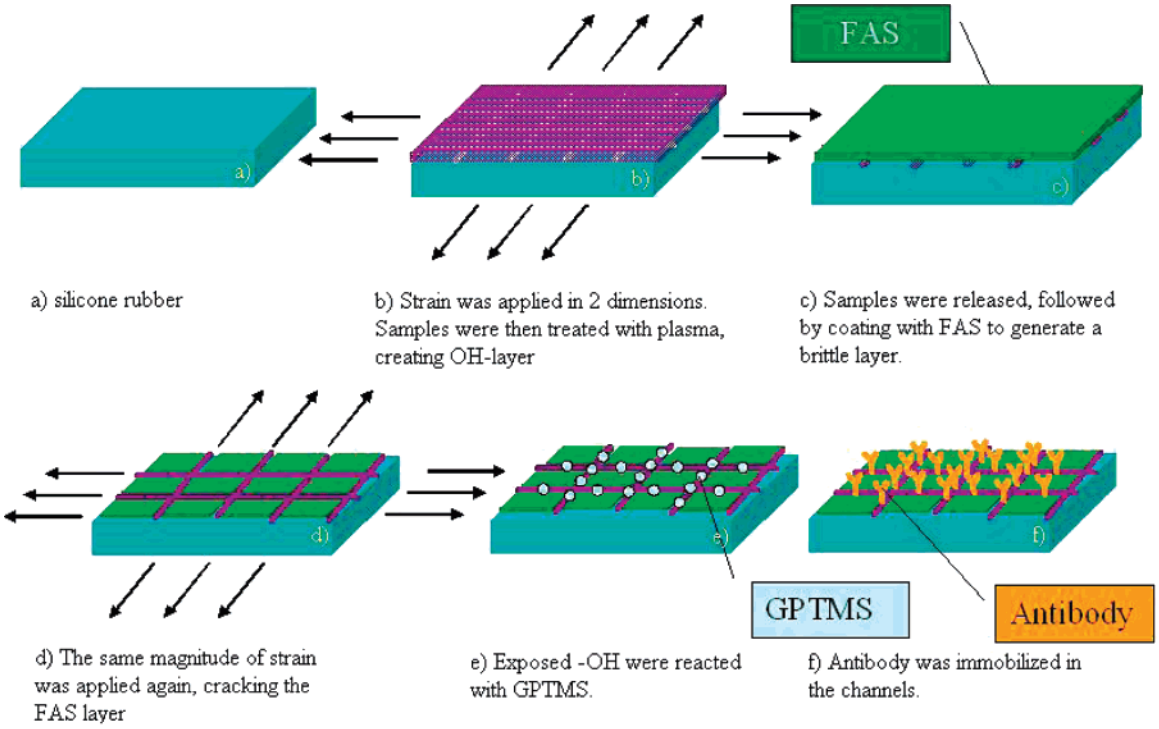

Figure 1. Schematic diagram of antibody-immobilized cracked SiR.

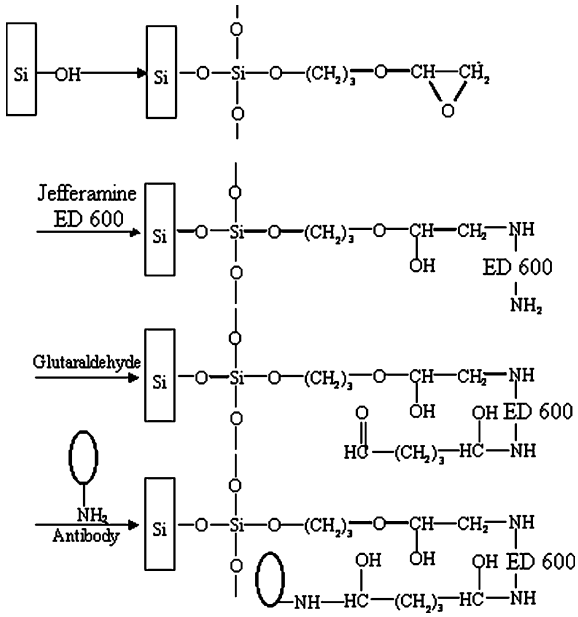

Figure 2. Reaction scheme showing the immobilization of antibody on silicone through covalent bonding with involving Jefferamine ED 600.

in both one and two dimensions by thin-film cracking and then *Escherichia coli* k99 pilus antibodies were covalently immobilized in the channels. Also, trichloro(1H,1H,2H,2H-perfluoroctyl)silane was coated on the substrates to generate nonadherant surfaces. Atomic force microscopy (AFM) and optical microscopy were used to characterize the distribution and size of pattern. Specificity and sensitivity of immobilized antibody were evaluated by enumerating bacteria using scanning electronic microscopy (SEM).

Materials and Experiment

Materials. Silastic silicone (0.010 in., gloss/gloss) was purchased from Specialty Manufacturing, Inc. (Saginaw, MI). Poly(dimethylsiloxane) (PDMS) base and curing agent (Sylgard 184) were obtained from Dow Corning (Midland, MI). Monoclonal antibody, *Escherichia coli* K99 pilus, was purchased from Fitzgerald Industries International, Inc. (Concord, MA). (3-Glycidyloxypropyl)trimethoxysilane (GPTMS), trichloro(1*H*,1*H*,2*H*,2*H*-perfluoroctyl)silane (97%) (FAS), glutaraldehyde, and phosphate-buffered saline (PBS: 136 mM NaCl, 2.68 mM KCl, 10.1 mM Na_2PO_4, and 1.37 mM KH_2PO_4, pH = 7.5) were purchased from Sigma (St. Louis, MO). Jeffamine ED-600 (polyether diamines based on a predominantly polyethylene oxide backbone) were provided by Huntsman Co. (Houston, TX). Toluene, ethanol, butanol, and dioxane were obtained from Fisher Scientific (Pittsburgh, PA). Water was purified with a Barnstead Nanopure system to a resistivity higher than 18 MΩ cm (Dubuque, IA). All chemicals were used without further purification.

Cultures. *E. coli* K99 ATCC 31619 were cultured at 37 °C in Trypticase soy agar (Becton Dickinson and Company, MD) and stored at 4 °C. After inoculation, bacteria from one colony from the plate were grown in Trypticase Soy Broth (Becton Dickinson and Company, MD) at 37 °C with a shaker speed of 150 rpm and then harvested in the mid-exponential growth phase. *E. coli* K12 JM109 (New England Biolabs, Beverly, MA) were grown under the same conditions using Luria-Broth (LB) Miller (EM Science, Gibbstown, NJ).

Preparation of Parallel and Crisscrossing Pattern. The procedures of making parallel and crisscrossing patterns are illustrated in Figure 1. Silicone sheets were cut into 25 mm × 40 mm × 0.254 mm (W × L × H) slabs in parallel samples and subjected to tensile strains, from 20, 40, 60, and 80%, using a custom-built manual stretcher at a constant strain rate of 1% s^{-1}. While in a stretched position, samples were oxidized by plasma (PDC-3XG, Harrick Scienfic Corporation, Ossining, NY) for 5 min under vacuum. This treatment removes surface methyl groups and leaves siloxyl groups on the surface with similar chemistry to the hydroxyl groups of the native oxide surface, providing the monofunctional groups for the silanization reaction to occur. Subsequently, the stress was relieved, and the surface

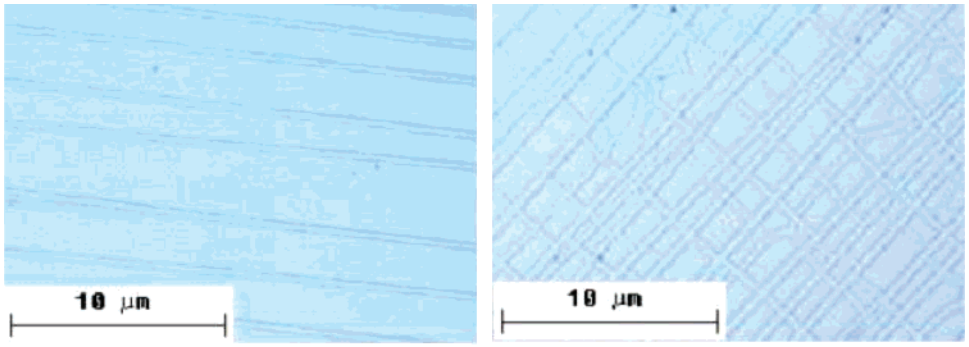

Figure 3. Optical microscopy images on the mold of stretched silicone samples in (a) one dimension and (b) two dimensions under 40% tensile strain.

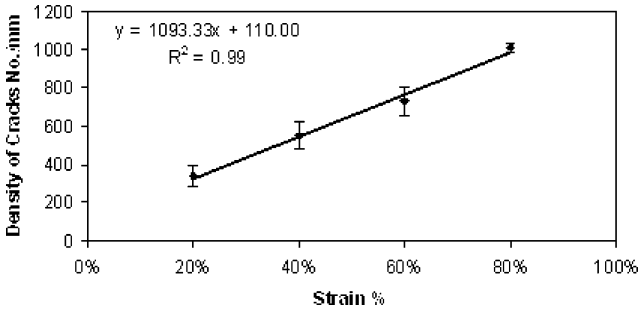

Figure 4. A relation between the density of cracks on stretched silicone samples and the applied tensile strain.

was silanized with FAS at 10^{-3} Torr and room temperature for 5 min by placement into a sealed chamber with a glass petri dish filled with FAS. The samples were maintained in the sealed chamber with the FAS for an additional 4 h at 0.3 Torr. Strains were applied on FAS-coated silicone samples again to generate an array of parallel or crisscrossing patterns in the coated layers. The cracks exposed at this time do not have a FAS coating; rather, the exposed crack surfaces had been oxygenated using plasma. As a result, the next silanization reaction can only occur on the exposed crack surfaces.

Generation of a crisscrossing pattern (90 mm × 90 mm × 0.254 mm for crisscrossing samples) followed the same procedures as for parallel patterns, except the stretching were made in two directions synchronously.

Preparation of Antibody Pattern with Covalent Immobilization. The process of antibody immobilization is shown in Figure 2. First, patterned silicone substrates were loaded in a sealed chamber while stretched to be silanized by GPTMS. In this step, either chemical vapor deposition (CVD) or a chemical solution method was utilized.

As for CVD silanization, the GPTMS coating was formed by chemical vapor deposition for 6 h at room temperature with GPTMS at 10^{-3} Torr then maintained in the sealed chamber for an additional 12 h. For the chemical solution method, samples were put in 1.5 wt % GPTMS/anhydrous toluene solution at 65 °C for 2 h followed by washing with toluene several times. The process of silanization in chemical solution results in a permanent patterns even after the silicone substrates were released from tensile strain.

Second, the GPTMS coated silicone pattern was activated by reacting with Jeffamine ED-600 (J600) in dioxane at 80 °C for 8 h. After rinsing copiously with dioxane and DI water, the substrates were then modified by incubating in 2.5% glutaraldehyde solution for 2 h at room temperature. Antibodies were immobilized on the aldehyde-reactive modified substrates by reaction overnight with K99 pilus IgG (0.1 mg/mL in PBS, pH 7.4) at room temperature. The antibody pattern samples were then washed with PBS and stored at 4 °C for further use.

Pattern Characterization. To characterize the crack patterns, PDMS molds of the silicone surfaces were made for optical microscopy measurement.[12] In brief, PDMS liquid was poured on FAS-silanized silicone while stretched. Then samples were cured in an oven at 60 °C for 3 h. Solid PDMS molds were peeled off from the stretched silicone substrates and examined by optical microscopy. The function of FAS in this step is to aid in releasing of the cured PDMS, which has the reverse geometry of the stretched patterns.

The profiles of the released silicone substrates were imaged by AFM. A Nanoscope IV-Dimension 3100 scanning probe microscope (Veeco Instrument, Santa Barbara, CA) was employed to measure the surface topography under tapping mode. The cantilever, with silicon tip (Nano Technology Instruments, Moscow, Russia), was oscillated at a frequency around 255 kHz. Tips were cleaned with ethanol and illuminated under UV light from a fiber optical illuminator (Dolan-Jenner Industries, Inc., Lawrence, MA) before use.

Evaluation of Antibody Specificity by SEM. Microscopic images of *E. coli* captured by pattern-immobilized antibodies were obtained using a Hitachi scanning electron microscope (S-2400, Hitachi). *E. coli* K99, collected in the mid-exponential growth phase, were diluted with Trypticase Soy Broth (or LB broth for *E. coli* JM109) to a concentration of 2×10^8 CFU/mL. In the specific detection studies, 5 mL of *E. coli* solution was incubated with each pattern-immobilized antibody substrate in a 50-mL conical tube (Becton Dickinson Labware, Franklin Lakes, NJ) at 37 °C with a shaker speed of 150 rpm for 10 min. The same procedures were employed in response time tests except the incubation time periods were varied.

After incubation with bacteria, samples were washed with LB broth and DI water several times in order to remove unbounded bacteria. Then, the samples were fixed with 2.5 vol % glutaraldehyde in 0.1 M PBS solution for at least 30 min and briefly rinsed with DI water and air dried. The samples were glued on mounts with silver conductive paint (Hatfield, PA) and then air-dried for at least 2 h. Specimens were sputter-coated with gold using an Ernest sputter coater (Latham, NY) at 50 mA for 25 s. SEM images of 10 randomly selected areas were taken under 4000× magnification at 25 kV.

Results and Discussion

Although fabrication of patterns by thin-film cracking has been widely studied,[12,26−28] no study has been done on covalent immobilization of protein on cracking patterns. In this study, we focus on using thin-film cracking to fabricate covalent pattern-immobilized anti-*E. coli* K99 pili patterns. Because of

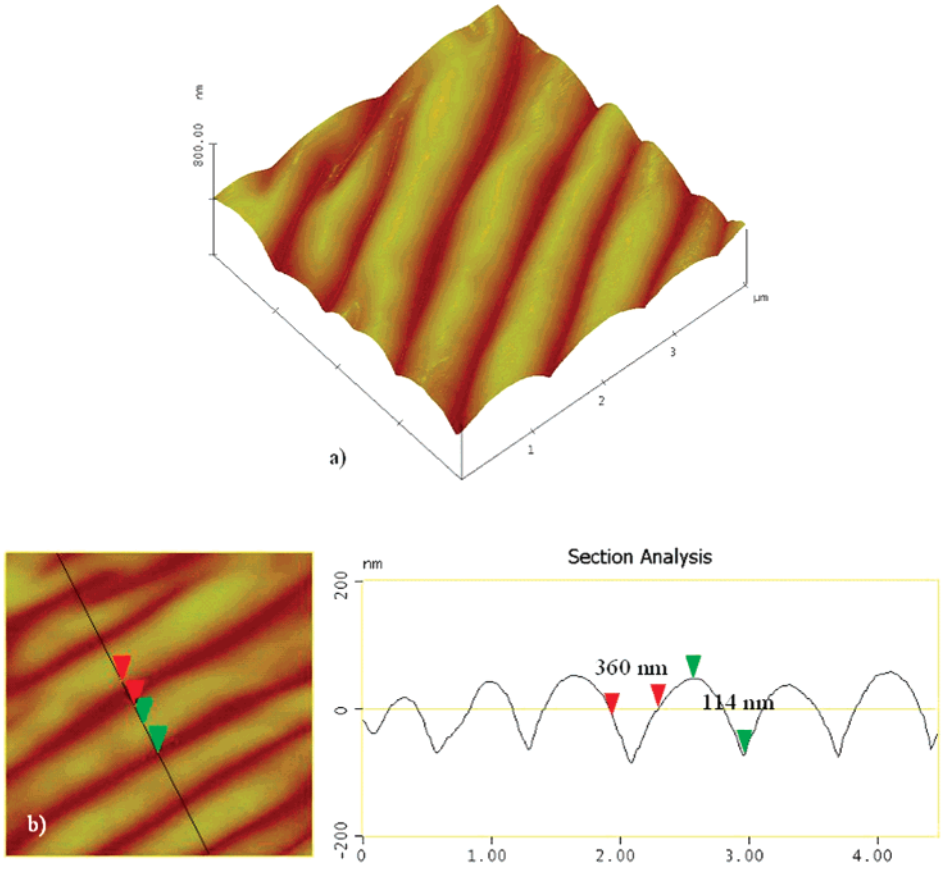

Figure 5. AFM topography of released patterns after applied 40% tensile strain. Samples were taken in ambient air using ultrasharp silicon NSG cantilevers with a resonance frequency of about 300 kHz. Tapping mode was used with a 0.5-Hz scan rate. The scan size was 4 μm × 4 μm.

dimension of crack patterns created by different approaches, optical microscopy was used to characterize the profile of pattern fabricated by solution approach, while AFM was applied to mapping the pattern generated by CVD method. Representative images of each approach series were presented.

Profile of Patterns: Solution Approach. Figure 3 shows the distribution of crack patterns on silicone under 40% tensile strain in one dimension (Figure 3a) and two dimensions (Figure 3b) using optical microscopy for those samples prepared using the solution-based silanization process. While the crack patterns on the substrate were not consistently uniform, the patterns appear parallel. Formation of a parallel pattern can be attributed to the differences in mechanical properties between the elastic silicone substrate and the more rigid FAS thin film layer. Thus, a uniaxial tensile strain can generate a parallel pattern in a direction perpendicular to that of the applied strain.

The average crack density, defined as number of cracks per mm^2 of surface, under various one-dimension tensile strains is shown in Figure 4. It is clear that the formation of the pattern is controlled and reproducible in terms of average crack density. The average crack density increased from 300/mm^2 at 20% tensile strain to 1000/mm^2 at 80% tensile strain. The increase in crack density with tensile strain is consistent with published observations of thin-film cracking.[12,29] It should be noted that, by the solution method, the spacing between cracks (~3 μm) and crack width (0.5 μm) are significantly larger than those obtained from the CVD approach.

Profile of Patterns: CVD Approach. Figure 5a shows a typical 3-D AFM image of a sample prepared using the CVD-based silanization process after the substrate was released from 40% tensile strain. Figure 5b shows a corresponding cross-section profile that reveals ~360 nm width and ~114 nm depth

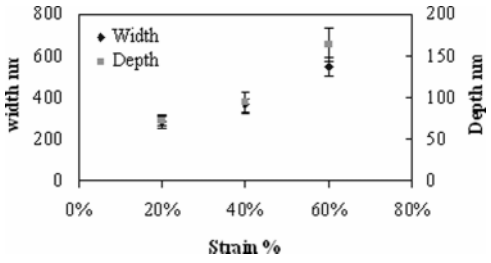

Figure 6. A relation between the width and depth of released patterns and the applied tensile strain (40%).

of the cracks. This relaxed substrate also displays "pile-up"[12] or "bulging"[30] features at the edge of cracks, which was also observed by Zhu et al.[12] and Tan et al.[30] In low-modulus and incompressible materials,[12] the elongation in the *x* direction results in an expansion in the *z* and *y* directions after the elongation is released due to the Poission's ratio.[31,32] The "bulging" or "pile up" effect is even stronger in our system since there is a mismatch in elastic constant between soft substrates and thin film coating, and substrates undergo additional constraint from the upper coated film.

Figure 6 shows the width and depth of the pattern generated by CVD approach with different applied tensile strains. The elastic constant of the FAS thin film layer formed on the substrates is significantly lower than the bulk materials; thus even 20% tensile strain generates a channel of about 250 nm in width and 75 nm in depth. When the applied tensile strain increases to 60%, the width and depth of cracks were 500 and 150 nm, respectively. Both the width and depth increased by a similar extent when the tensile strain was increased.

One prerequisite for the fabrication of covalently immobilized anti-*E. coli* K99 pili patterns is the control of the pattern density

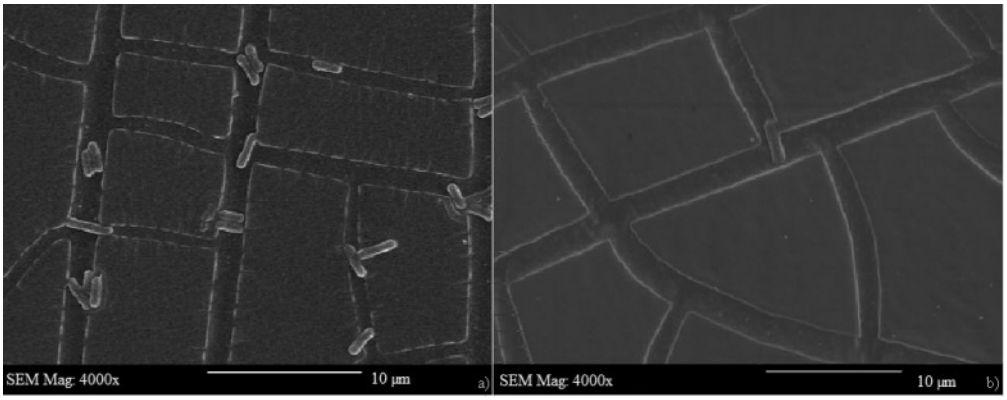

Figure 7. SEM images of antibody pattern surfaces exposed to (a) specific strain *E. coli* K99 and (b) nonspecific strain *E. coli* JM109 for 10 min.

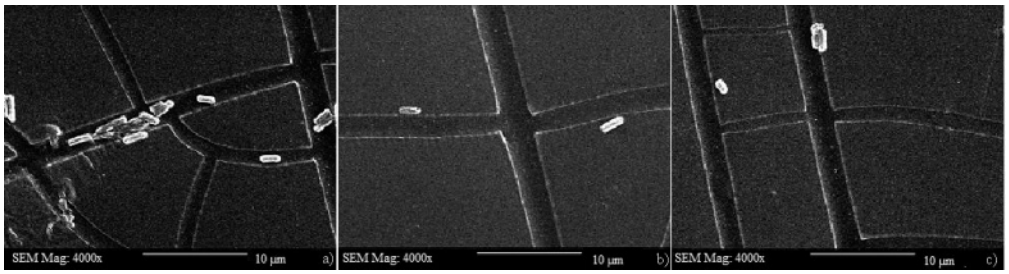

Figure 8. SEM images of antibody pattern surfaces exposed to (a) specific strain *E. coli* K99; non-antibody pattern surfaces on (b) *E. coli* K99 and (c) *E. coli* JM109 for 10 min.

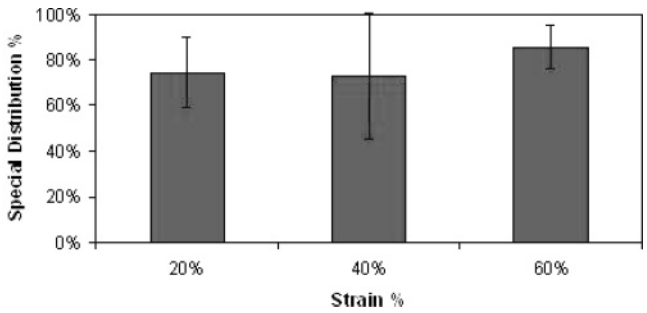

Figure 9. Quantitative comparison of special distribution of adherent bacteria on antibody pattern under different applied tensile strain.

and its geometry. In the present study, the crack distribution was not very uniform (Figures 3 and 5) with two possible explanations. First, maintaining uniform crack spacing on a nanoscale is a challenge because of the driving force between the two strain fields.[33] The other reason can be attributed to local inhomogeneities, complex microstructures, and plastic deformation exhibited in real materials.[28] Similar nonuniform cracking patterns were also reported by Heinrich et al.,[28] which showed an increase in the tensile strain can cause the existing cracks to grow and to generate new primary-type crack nucleates. As a result, the defects in the bulk substrates were the potential nucleates for crack formation, which may explain the inhomogeneous patterns.

The crack profiles show a good correlation with different applied tensile strains. The width of cracks ranges from ~250 to ~600 nm with the CVD method and varies from ~900 to ~2000 nm with the solution method. The crack widths observed in this study are comparable to the values reported by others (120−3200 nm[12]). After release from 20% tensile strain, the crack width of samples is similar (~250 nm) to Zhu et al. However, greater widths were obtained on the molded patterns (~2500 nm) in their work (at 20% strain) compared to those (~1300 nm) obtained by the solution method in this study. The difference can possibly be attributed to the higher strain rate used in their study (10% s^{-1}) as compared to this work (1% s^{-1}).

Specificity of Immobilized Antibodies. Our previous research has demonstrated that GPTMS can react with the amine group of antibodies.[24,34,35] Moreover, by introducing a flexible, long chain spacer in the antibody immobilization process, one can significantly reduce the steric interference.[36,37] Thus, in the antibody immobilization process for this work, Jeffamine ED-600 (J600) was used to improve the binding efficiency of immobilized antibody and reduce the steric hindrance from the substrates.[35]

The specificity of immobilized antibodies was evaluated by two approaches with samples fabricated through solution method. First, two different *E. coli* strains, *E. coli* K99 and *E. coli* JM109, were exposed to the antibody-immobilized surfaces respectively. Since the immobilized antibody was specific to the K99 bacterial strain, it was hypothesized that this strain would be preferentially observed on the surface. Control experiments were performed by incubation with a solution of *E. coli* JM109 solution, which is nonspecific to the K99-pili antibody.

Figure 7 shows representative images of crisscrossing pattern immobilized anti-*E. coli* K99 pili (after 60% tensile strain) after 10 min incubation with 2×10^8 CFU/mL K99 (Figure 7a) and JM109 (Figure 7b) bacteria. The specificity of anti-K99 pili differed dramatically between different bacterial strains on the same substrates. For example, in the presence of anti-*E. coli* K99 pili antibody, the number of K99 bacteria observed is almost 10 times the number of JM109 observed under comparable circumstance. The majority of K99 bacteria attached on anti-*E. coli* K99 pili antibody pattern were located within the channels, while few were observed in the nonadhesive regions. The SEM result is direct evidence that the immobilized antibody retains the bioactivity after covalent bonding (Figure 7a). In the nonspecific strain test, there were few JM109 observed

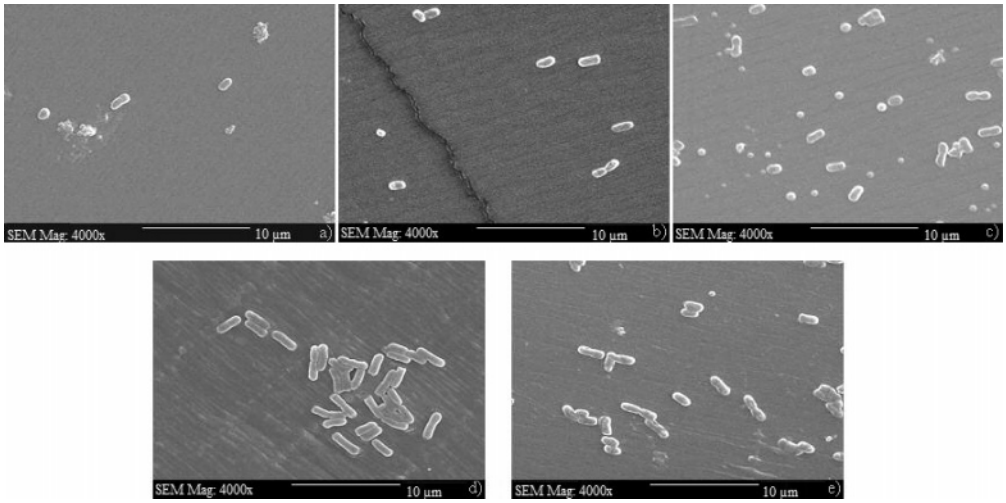

Figure 10. SEM images of antibody pattern surfaces exposed to specific strain *E. coli* K99 for (a) 1, (b) 2, (c) 5, (d) 10, and (e) 15 min.

within the channels, which also demonstrates the specificity of antibodies after immobilization.

To distinguish the specific detection ability of anti-*E. coli* K99 pili pattern from adhesion of the surfaces, a second strategy was to compare the detection of bacteria on both anti-*E. coli* K99 pili patterned and blank patterned substrates. As shown in Figure 8a, viability of K99 along the channels was confirmed again with anti-*E. coli* K99 pili patterns. On the other hand, very few bacteria, whether K99 (Figure 8b) or JM109 (Figure 8c) were observed on blank patterned substrates. Interestingly, for the few bacteria observed, both bacteria strains tend to spread and align near the edges of the cracks but not within the crack (parts b and c of Figure 8). As opposed to the anti-*E. coli* K99 pili patterned substrates, the surfaces without antibody exhibited no specificity.

Comparison was also made of the special distribution of adherent bacteria on the surface based on the SEM images obtained from different locations. The number of bacteria observed adjacent to and within cracks divided by the total number of attached bacteria was computed. As shown in Figure 9, 74−86% of the bacteria were associated with cracks, which indicate that specific antibody−cell interactions is predominated. In terms of sensor behavior, "false positive" or background signal would be associated with the nonspecific adherences.

Minimizing the background signal is another important feature of the incorporation of antibody pattern for sensing substrates. A bacterial- and cell-resistant surface was obtained by silanized with FAS,[23−25] which also permitted the formation of the thin film with a mismatched elastic modulus from the substrates. As mentioned previously the selection of FAS was based on previous results. Nonadhesive properties depend on cell or bacterial type and the interaction between them.[17,24] For example, Pluronic can be employed to block the nonspecific protein adsorption.[12] For different detected analytes, choosing the appropriate nonadhesive coating layers is important. With the FAS coating, some chemicals can physisorbed on it directly, such as albumin and Pluronic, which provides a versatile way of tailoring non-adhesive construction.

Response Time. Anti-*E. coli* K99 pili antibody patterns substrates generated from the CVD approach were incubated in K99 bacteria solution for various time periods from 1 min up to 60 min. As illustrated in Figure 10, the amount of detected bacteria increased with the exposure time.

The amount of K99 observed under various incubation times are illustrated in Figure 11. From the first 10 min, a gradual increase occurs and approaches a saturated surface around 15 min which can be fitted with Langmuir isotherm.

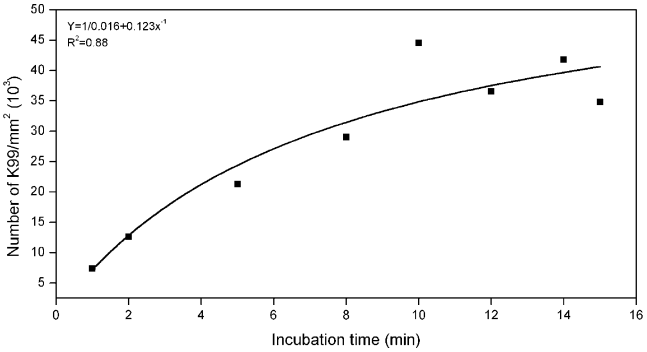

Figure 11. A relation between the number of detected *E. coli* K99 on antibody pattern surfaces as a function of incubation time.

Conclusion

The protocol presented in this study provides a versatile technique to fabricate chemically immobilized protein patterns by thin-film cracking. The pattern width can be varied from ∼250 to ∼2000 nm, in which the loading rates may be a factor that influences the pattern geometry. Covalently coupled antibody in the channel retains its specificity, and the antibody pattern can reach the saturated status in 10 min. Overall, the simplicity of this pattern fabrication technique combined with the stable protein bonding strategy may facilitate the use of protein microarrays in sensing applications.

Acknowledgment. We thank Dr. Gina Shreve and Dr. Guangzhao Mao, of the Chemical Engineering and Material Science Department of Wayne State University, for their help in using the equipment. Financial support of the research by TACOM (Contract No. DAAE07-03-C-L140) is gratefully acknowledged.

References and Notes

(1) Blume-Jensen, P.; Hunter, T. *Nature* **2001**, *411*, 355−365.
(2) Liotta, L. A.; Kohn, E. C. *Nature* **2001**, *411*, 375−379.
(3) Velev, O. D.; Kaler, E. W. *Langmuir* **1999**, *15*, 3693−3698.
(4) Kramer, S.; Fuierer, R. R.; Gorman, C. B. *Chem. Rev.* **2003**, *103*, 4367−4418.
(5) Frost, F.; Rauschenbach, B. *Appl. Phys. A* **2003**, *77*, 1−9.
(6) Younkin, R.; Berggren, K. K.; Johnson, K. S.; Prentiss, M.; Ralph, D. C.; Whitesides, G. M. *Appl. Phys. Lett.* **1997**, *71*, 1261−1263.

(7) Forster, S.; Antonietti, M. *Adv. Mater.* **1998**, *10*, 195−217.
(8) Fasolka, M. J.; Mayes, A. M. *Annu. Rev. Mater. Res.* **2001**, *31*, 323−355.
(9) Geissler, M.; Xia, Y. N. *Adv. Mater.* **2004**, *16*, 1249−1269.
(10) Tseng, A. A.; Chen, K.; Chen, C. D.; Ma, K. J. *IEEE Trans.* **2003**, *26*, 141−149.
(11) Bowden, N. B.; Weck, M.; Choi, I. S.; Whitesides, G. M. *Acc. Chem. Res.* **2001**, *34*, 231−238.
(12) Zhu, X. Y.; Mills, K. L.; Peters, P. R.; Bahng, J. H.; Liu, E. H.; Shim, J.; Naruse, K.; Csete, M. E.; Thouless, M. D.; Takayama, S. *Nat. Mater.* **2005**, *4*, 403−406.
(13) Elbahri, M.; Rudra, S. K.; Wille, S.; Jebril, S.; Scharnberg, M.; Paretkar, D.; Kunz, R.; Rui, H.; Biswas, A.; Adelung, R. *Adv. Mater.* **2006**, *18*, 1059.
(14) Mani, S.; Saif, T.; Han, J. H. *IEEE Trans.* **2006**, *5*, 138−141.
(15) Zhao, Z. B.; Hershberger, J.; Yalisove, S. M.; Bilello, J. C. *Thin Solid Films* **2002**, *415*, 21−31.
(16) Weimer, B.; Walsh, M.; Wang, X. *J. Biochem. Biophys. Methods* **2000**, *45*, 211−219.
(17) Nelson, C. M.; Chen, C. S. *FEBS Lett.* **2002**, *514*, 238−242.
(18) Luk, Y. Y.; Kato, M.; Mrksich, M. *Langmuir* **2000**, *16*, 9604−9608.
(19) Chen, C. S.; Mrksich, M.; Huang, S.; Whitesides, G. M.; Ingber, D. E. *Science* **1997**, *276*, 1425−1428.
(20) McDevitt, T. C.; Angello, J. C.; Whitney, M. L.; Reinecke, H.; Hauschka, S. D.; Murry, C. E.; Stayton, P. S. *J. Biomedical Mater. Res.* **2002**, *60*, 472−479.
(21) Razatos, A.; Ong, Y.; Boulay, F.; Elbert, D.; Hubbell, J.; Sharma, M.; Georgiou, G. *Langmuir* **2000**, *16*, 9155−9158.
(22) Marsh, L. H.; Alexander, C.; Coke, M.; Dettmar, P. W.; Havler, M.; Nevell, T. G.; Smart, J. D.; Timmins, B.; Tsibouklis, J. *Int. J. Pharm.* **2003**, *251*, 155−163.
(23) Cao, T.; Tang, H. Y.; Liang, X. M.; Wang, A. F.; Auner, G. W.; Salley, S. O.; Ng, K. Y. S. *Biotechnol. Bioeng.* **2006**, *94*, 167−176.
(24) Tang, H. Y.; Wang, A. F.; Liang, X. M.; Cao, T.; Salley, S. O.; McAllister, J. P.; Ng, K. Y. S. *Colloids Surf., B* **2006**, *51*, 16−24.
(25) Patel, K. R.; Tang, H. Y.; Grever, W. E.; Ng, K. Y. S.; Xiang, J. M.; Keep, R. F.; Cao, T.; McAllister, J. P. *Biomaterials* **2006**, *27*, 1519−1526.
(26) Lacour, S. P.; Wagner, S.; Huang, Z. Y.; Suo, Z. *Appl. Phys. Lett.* **2003**, *82*, 2404−2406.
(27) Jones, J.; Lacour, S. P.; Wagner, S.; Suo, Z. G. *J. Vacuum Sci. Technol. A* **2004**, *22*, 1723−1725.
(28) Heinrich, M.; Gruber, P.; Orso, S.; Handge, U. A.; Spolenak, R. *Nano Lett.* **2006**, *6*, 2026−2030.
(29) Shenoy, V. B.; Schwartzman, A. F.; Freund, L. B. *Int. J. Fracture* **2000**, *103*, 1−17.
(30) Tan, L.; Ouyang, Z. Q.; Liu, M. Z.; Ell, J.; Li, H.; Hu, J.; Patten, T. E.; Liu, G. Y. *J. Phys. Chem. B* **2006**, *110*, 23315.
(31) Lakes, R. *Science* **1987**, *235*, 1038−1040.
(32) Russell, T. P. *Science* **2002**, *297*, 964−967.
(33) Mani, S.; Saif, T. M. *Appl. Phys. Lett.* **2005**, *86*, -.
(34) Bilitewski, U. *Anal. Chim. Acta* **2006**, *568*, 232−247.
(35) Cao, T.; Wang, A. F.; Liang, X. M.; Tang, H. Y.; Auner, G. W.; Salley, S. O.; Ng, K. Y. S. *Biotechnol. Bioeng.* **2007**, *98*, 1109−1122.
(36) Soltys, P.; Etzel, M. *Biomaterials* **2000**, *21*, 37−48.
(37) Tozzi, C.; Salomone, A.; Giraudi, G.; Anfossi, L.; Baggiani, C.; Giovannoli, C. *Anal. Chim. Acta* **2004**, *510*, 153−161.